NRC·CNRC

NRC Publications Archive
Archives des publications du CNRC

Single hole spin relaxation probed by fast single-shot latched charge sensing

Bogan, Alex; Studenikin, Sergei; Korkusinski, Marek; Gaudreau, Louis; Zawadzki, Piotr; Sachrajda, Andy; Tracy, Lisa; Reno, John; Hargett, Terry

This publication could be one of several versions: author's original, accepted manuscript or the publisher's version. / La version de cette publication peut être l'une des suivantes : la version prépublication de l'auteur, la version acceptée du manuscrit ou la version de l'éditeur.
For the publisher's version, please access the DOI link below./ Pour consulter la version de l'éditeur, utilisez le lien DOI ci-dessous.

Publisher's version / Version de l'éditeur:
https://doi.org/10.1038/s42005-019-0113-0
Communications Physics, 2, 1, 2019-02-18

NRC Publications Archive Record / Notice des Archives des publications du CNRC :
https://nrc-publications.canada.ca/eng/view/object/?id=e45db34a-b597-42a5-af5f-9d0a95da0cb7
https://publications-cnrc.canada.ca/fra/voir/objet/?id=e45db34a-b597-42a5-af5f-9d0a95da0cb7

Access and use of this website and the material on it are subject to the Terms and Conditions set forth at
https://nrc-publications.canada.ca/eng/copyright
READ THESE TERMS AND CONDITIONS CAREFULLY BEFORE USING THIS WEBSITE.

L'accès à ce site Web et l'utilisation de son contenu sont assujettis aux conditions présentées dans le site
https://publications-cnrc.canada.ca/fra/droits
LISEZ CES CONDITIONS ATTENTIVEMENT AVANT D'UTILISER CE SITE WEB.

Questions? Contact the NRC Publications Archive team at PublicationsArchive-ArchivesPublications@nrc-cnrc.gc.ca. If you wish to email the authors directly, please see the first page of the publication for their contact information.

Vous avez des questions? Nous pouvons vous aider. Pour communiquer directement avec un auteur, consultez la première page de la revue dans laquelle son article a été publié afin de trouver ses coordonnées. Si vous n'arrivez pas à les repérer, communiquez avec nous à PublicationsArchive-ArchivesPublications@nrc-cnrc.gc.ca.

National Research Council Canada | Conseil national de recherches Canada

Canada

COMMUNICATIONS PHYSICS

ARTICLE

https://doi.org/10.1038/s42005-019-0113-0 OPEN

Single hole spin relaxation probed by fast single-shot latched charge sensing

Alex Bogan[1,2], Sergei Studenikin[1,2], Marek Korkusinski[1], Louis Gaudreau[1], Piotr Zawadzki[1], Andy Sachrajda[1], Lisa Tracy[3], John Reno[4] & Terry Hargett[4]

Hole spins have recently emerged as attractive candidates for solid-state qubits for quantum computing. Their state can be manipulated electrically by taking advantage of the strong spin-orbit interaction (SOI). Crucially, these systems promise longer spin coherence lifetimes owing to their weak interactions with nuclear spins as compared to electron spin qubits. Here we measure the spin relaxation time T_1 of a single hole in a GaAs gated lateral double quantum dot device. We propose a protocol converting the spin state into long-lived charge configurations by the SOI-assisted spin-flip tunneling between dots. By interrogating the system with a charge detector we extract the magnetic-field dependence of $T_1 \propto B^{-5}$ for fields larger than $B = 0.5$ T, suggesting the phonon-assisted Dresselhaus SOI as the relaxation channel. This coupling limits the measured values of T_1 from ~400 ns at $B = 1.5$ T up to ~60 μs at $B = 0.5$ T.

[1] Security and Disruptive Technologies Research Centre, National Research Council of Canada, Ottawa, ON K1A0R6, Canada. [2] Department of Physics and Astronomy, University of Waterloo, Waterloo N2L3G1 ON, Canada. [3] Sandia National Laboratories, Albuquerque, NM 87185, USA. [4] Center for Integrated Nanotechnologies, Sandia National Laboratories, Albuquerque, NM 87185, USA. Correspondence and requests for materials should be addressed to S.S. (email: Sergei.Studenikin@nrc-cnrc.gc.ca)

Coherence of solid-state spins is of crucial importance in the context of their utilization in quantum computation and communication[1–3]. This property is quantified by the spin relaxation time T_1 and the decoherence time T_2^*[3]. While both of them are essentially material parameters, T_2^* can be extended dynamically by refocusing techniques[4]. On the other hand, $1/T_1$ measures the spin relaxation rate from an arbitrary linear superposition to the ground state, by which the quantum information is lost irreversibly. Extending T_1 is thus essential. Here, solid-state holes offer an advantage, as they interact much weaker than the electrons with the nuclei in the crystal lattice[5].

Two mechanisms of the spin relaxation process in quantum dots have been identified[3,6]. The first involves flip–flop interactions with nuclear spins of the crystal lattice and is active at magnetic fields B up to several mT. The resulting T_1 was measured to be 10–100 ns at very small fields for electrons in gated GaAs quantum dots[3], rising to ~70 μs at $B = 100$ mT[7]. It can be radically enhanced by moving to ^{28}Si samples where nuclear spins are absent[8]. However, GaAs hole spins have a competitive edge, since their hyperfine interaction strength in bulk was predicted[9–12] and measured[13–15] to be an order of magnitude weaker than that of the electrons. This suppression translates into improved values of T_1, reaching 1 ms for holes in InGaAs samples[16,17].

In the second mechanism, dominant at higher magnetic fields, the spin relaxation occurs via the phonon-mediated spin–orbit interaction (SOI). Crossover into this regime occurs when the spin Zeeman energy exceeds the hyperfine interaction strength[18] and is marked by a large increase of T_1[3]. In Si/SiGe dots, T_1 was reported to reach ~3 s at $B = 1$–2 T[19,20]; in GaAs systems at similar fields $T_1 \sim 1$ s[3,21], whereas in InGaAs $T_1 \sim 20$ ms at $B = 2$ T[22] and $T_1 \sim 1$ ms at $B = 5$ T[23]. The trend follows the strength of the SOI, which is weaker in centrosymmetric materials such as Si, and strongest in III–V In-based systems. The importance of the phonon component is revealed in the dependence of T_1 on the magnetic field, as the increasing spin Zeeman energy tracks the increasing phonon density of states. The dependence of $T_1 \propto B^{-5}$ was predicted theoretically[24,25] and confirmed experimentally in GaAs quantum dots[3,22,23,26–28], revealing values of $T_1 \sim 100$ μs at $B \sim 10$ T.

For hole spins, theory also predicts a decrease of T_1 with increasing magnetic field, with $T_1 \propto B^{-5}$ for the Dresselhaus SOI, or $T_1 \propto B^{-9}$ for the Rashba SOI[29,30]. Moreover, the exact functional relationship depends on the structural properties of the dots, such as size, thickness, shape, and strain, characteristic for the strong SOI experienced by holes in solids[31–33]. However, there has been little systematic experimental analysis of T_1 in p-type quantum dots at higher magnetic fields. Measurements in Ge/Si samples suggest T_1 of hundreds of microseconds[34] to sub-microsecond values[35] at $B \sim 1$ T. In the Ge hut wire system, values of tens to a hundred microseconds were recorded for magnetic fields from 0.5 T to 1.5 T[36]. T_1 times of several microseconds in hole Si Complementary Metal Oxide Semiconductor (CMOS) devices[37], and several nanoseconds in gated GaAs samples at similar fields[38] have been reported. Two-axis coherent control of the hole spin has been demonstrated both in the Ge hut sample[39] and in the Si dots[40]. With the exception of the Si device, however, all measurements mentioned above involved systems with several holes.

Here we report on the detailed experimental study of the single-hole T_1 as a function of the magnetic field. We show that, in the range of $B = 0.5$–1.5 T, T_1 changes from 60 μs down to 400 ns along the power law of $T_1 \propto B^{-5}$. This result, in agreement with theory[29,30], reveals the dominance of the Dresselhaus SOI in spin relaxation. Although our values of T_1 are lower than those for electrons in GaAs at similar fields, extrapolation to very small magnetic fields is consistent with previous optical measurements[16,17], showing holes to be superior (T_1 potentially in tens of milliseconds at $B \sim 100$ mT) owing to the reduced hyperfine interactions. We also report on the development of a technique to read out a single-hole spin qubit in one quantum dot by converting the spin state into a latched charge state in a secondary dot. Charge-latching techniques involving spin-to-charge mapping have been applied to a variety of qubits[41–44]. In the gated electronic double dot, the latching technique proposed by our group[42] involved the mapping of the spin of a singlet–triplet qubit onto the charge states differing by one electron charge, rather than by the charge distribution of different spin states. The technique relies on a long-lived (latched) nature of the ground and excited charge states allowing for a high-contrast charge sensor readout. The latched technique was used to demonstrate single-shot high-fidelity spin measurements[44,45] and to extend the sensitivity of the spin detection at large magnetic-field gradients[46]. The spin-to-charge conversion allows measuring T_1 by fitting the leakage current in the Pauli-blockaded state to a theoretical formula describing a relaxation cascade in the electron[3,19,27,47] or hole systems[34,35,37,38]. However, this technique cannot be used directly for our hole GaAs dot because of the strong spin-flip tunneling due to the SOI[48,49], resulting in the suppression of the spin blockade. Another approach utilizes the spin-selective time-resolved tunneling to leads[20,23,26,28]; however, the charge detection in our system is not sufficiently fast for high-fidelity sub-microsecond measurements. Instead, we propose a method of projective measurement of a single-hole spin utilizing fast resonant tunneling between dissimilar spin states in adjacent dots. This spin-flip tunneling is much weaker in electronic GaAs quantum dots but was recently reported to be strong in hole quantum dots in the single-hole[49] and two-hole regime[48]. We convert short-lived spin states into long-lived metastable charge states utilizing spin-selective, spin-flip resonant tunneling of a single hole between the dots of the lateral double dot. This enables single-shot measurements of spin states of a relaxing hole with timescales much faster than could be achieved by non-latching methods.

Results

Double-dot gated device confining a single hole. Our lateral double quantum dot (DQD) was defined by electrostatic gates on the surface of an undoped GaAs/AlGaAs heterostructure[48–50]. Figure 1a shows the gate layout of the device, with the two QD potential minima denoted as 1 and 2, respectively. The star denotes the DC-biased quantum point contact (QPC) utilized to measure the charge configurations of the system. The device is operated in the single-hole regime, i.e., with gate voltages V_L and V_R chosen to correspond to the regions of stability of the $(N_L, N_R) = (1, 0)$, $(0, 1)$, or $(0,0)$, as shown in Fig. 1b (N_i denotes the occupation of the ith dot). The magnetic field $\mathbf{B} = [0, 0, B]$ is applied in the direction perpendicular to the sample surface. Owing to a strong hole confinement in the growth direction of the system, the heavy and light hole subbands are separated by a substantial gap (~10 meV), resulting in a nearly pure heavy-hole character of the confined carriers. This is evidenced by a strong g-factor anisotropy, leading to a nearly zero effective g factor for the in-plane magnetic field, with $g^* \approx 1.35$ for the out-of-plane field[48]. However, the spin–orbit interaction is sufficiently strong to enable a spin-flip tunneling channel, with the characteristic matrix element being of the same order as that characterizing the usual spin-conserving tunneling process[48,49].

Measurement protocol. We extract T_1 by probing the relaxation process of the excited state $|L\Uparrow\rangle$ into the ground state $|L\Downarrow\rangle$ of the charge configuration (1,0), where $\Uparrow$ ($\Downarrow$) denotes the hole spin up

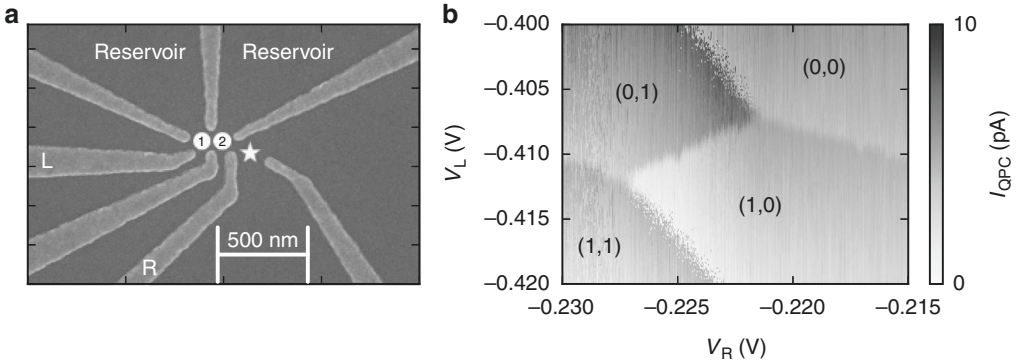

Fig. 1 Layout of the sample and charging diagram. **a** Scanning electron microscope image of the gate layout of the double quantum dot. Gates L (left) and R (right) are most strongly coupled to dots 1 and 2, respectively. **b** Charge stability diagram as a function of voltage on gates L and R, near the (1,0)/(0,1) charge transfer line

(down). The magnetic field opens the Zeeman gap $E_Z = g\mu_B B$ between the two spin states, with μ_B being the Bohr magneton and the effective hole g factor $g = 1.35$ in our system[48,49]. Since in our system the in-plane effective g factor is close to zero[48,49], our protocol is only sensitive to the out-of-plane component of the magnetic field. We map the spin state of the left dot onto the long-lived charge state of the right dot, which plays the role of the memory register. Its state can then be analyzed using the charge sensor. The use of the right dot as a long-lived, latched memory register is enabled by isolating it from the right lead, i.e., raising the right tunnel barrier to prevent the direct tunneling between the (0, 0) and (0, 1) charge states. The tunneling rate Γ_R between the right dot and the right lead can be measured in a transport measurement[49], and in our system it was ~2 Hz. On the other hand, the left dot is strongly coupled to the left lead (the tunneling rate $\Gamma_L \sim 100$ MHz). Moreover, the interdot barrier is set to enable the resonant tunnel coupling of order of ~0.2 μeV[49], giving the tunneling rate of ~50 MHz. The rate of the inelastic interdot tunneling, occurring when the right and left dot levels are off-resonance, is estimated at $\Gamma_C \sim 0.5$ MHz. By this arrangement, the charge state of the right dot is long-lived, while the left dot can be quickly emptied to the left lead by raising its energy above the Fermi level of the lead.

The left-dot spin states $|L\Uparrow\rangle$ and $|L\Downarrow\rangle$ are mapped respectively onto the charge states (0, 1) and (0, 0) of the latching memory register using the single-shot preparation and measurement protocol outlined in Fig. 2. The protocol involves applying a five-step voltage pulse $\Delta V_L(t)$ to the left gate along the profile shown in Fig. 2a. This pulse transfers the system among three points, T, R, and M, in the charging diagram of Fig. 2b, corresponding to the three phases of the sequence: transfer, relaxation, and measurement, respectively. The evolution of the state of the system at each voltage step is illustrated with diagrams c–j of Fig. 2.

The protocol begins with emptying the DQD, which requires clearing the latched memory. To this end, we visit the point R, in which both spin states of the left dot are lower in energy than those of the right dot, as depicted in Fig. 2c. By maintaining this alignment for 10 μs (i.e., long compared to the inelastic transfer rate Γ_C), we let the system relax into the (1, 0) charge configuration. Next, we pulse rapidly to the point M, placing the left-dot states at energy higher than those of the right dot or the Fermi level of the left lead, as shown in Fig. 2d. Owing to the asymmetry of the barriers, the hole is promptly ejected into the left lead and the system is cast in the charge configuration (0, 0).

In the third step, we pulse back to the point R, as shown in Fig. 2e and h. Here, a single-hole tunnel from the left lead into the left dot, occupying the $|L\Uparrow\rangle$ state with the probability $P_{L\Uparrow}(t = 0)$, and the $|L\Downarrow\rangle$ state with the probability $P_{L\Downarrow}(t = 0)$. This arrangement is maintained over time T_R, during which the spin relaxation takes place. At the end of this step, the probability $P_{L\Uparrow}(t = T_R) = P_{L\Uparrow}(t = 0)e^{-T_R/T_1}$, i.e., it decays exponentially with the rate defined by T_1. For further discussion, we consider two limiting cases of the spin state: $P_{L\Uparrow}(t = 0) = 0$ (Fig. 2e) and $P_{L\Uparrow}(t = 0) = 1$ (Fig. 2h).

The fourth step is the essence of our spin readout protocol. The system is positioned at the point T of the charging diagram, in which the spin-up state $|L\Uparrow\rangle$ is resonant with the spin-down state of the right dot (the memory register), as shown in Fig. 2f, i. These two states are coupled by the spin–orbit tunneling process, in which the charge is resonantly transferred between the dots with a spin flip[48,49]. No tunneling occurs if the state of the left dot is $|L\Downarrow\rangle$, as shown in Fig. 2f. However, if the left-dot state has a finite spin-up component, i.e., $P_{L\Uparrow}(T_R) > 0$, this component will tunnel resonantly into the right dot (Fig. 2i). As already mentioned, the rate of this resonant tunneling process is ~50 MHz. We maintain our system in this configuration for $T_T = 100$ ns. After this time the spin-up charge probability density $P_{L\Uparrow}(T_R)$ is split into the density $P_{L\Uparrow}(T_R + T_T)$ remaining on the state $|L_\Uparrow\rangle$ and the density $P_{R\Downarrow}(T_R + T_T)$ transferred onto the orbital $|R\Downarrow\rangle$ of the right dot. The probability of occupation of the $|L\Downarrow\rangle$ orbital, including any relaxation taking place during the transfer time, is now $P_{L\Downarrow}(T_R + T_T)$. We note that the possible small differences of the value of g-factor from one dot to another do not influence this spin-to-charge mapping process, as they can be compensated for by an appropriate choice of the gate voltage in this phase.

Having mapped the hole spin onto the charge configuration, we now proceed to the latching and readout step. As shown in Fig. 2g, j, we pulse the system to the point M, positioning the left-dot orbitals above the Fermi energy of the left lead. This ejects any charge residing in the left dot, while the charge state of the right dot remains latched. Figure 2g, j show, respectively, the states of the latched memory register in the limiting cases of $P_{L\Uparrow} = 0$ and $P_{L\Uparrow} = 1$. The former case corresponds to the memory state of (0, 0), while the latter corresponds to the state (0, 1), and these two charge configurations are distinguished by the QPC charge detector with high fidelity: for the state (0, 0) [(0, 1)], we expect a high [low] QPC current I_{QPC}. In reality, the measurement by the charge detector collapses the hole state, and detects the configuration (0, 1) with the probability $P_{01} = P_{R\Downarrow}(T_R + T_T)$. As we can see, the detection of this memory state is equivalent to the measurement of a finite spin-up component of the hole state at the end of the relaxation step. We note that the readout step takes place in the region of the charging diagram in which the ground-state configuration is (0, 0) (as indicated by the position of point M in the stability diagram in Fig. 2b). This makes the latched

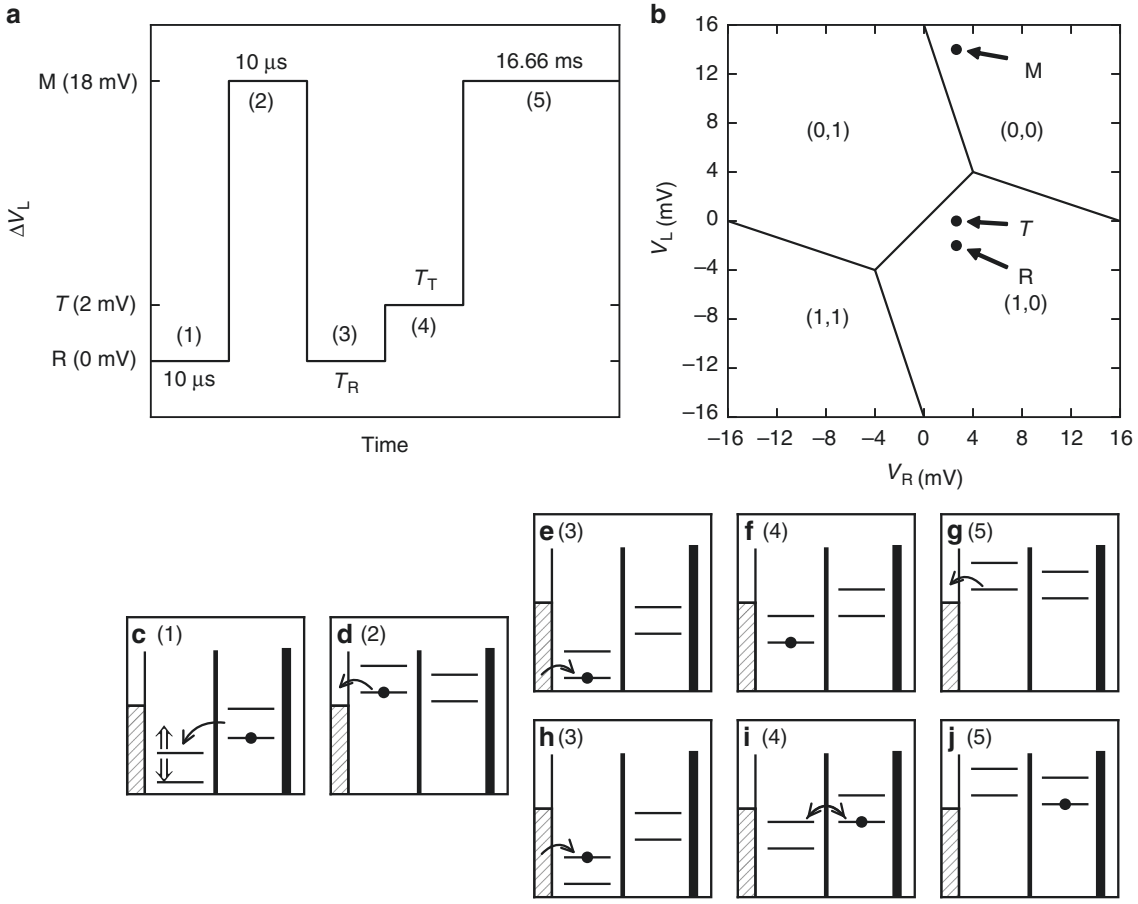

Fig. 2 Spin readout protocol. **a** Single cycle of the pulse sequence applied to gate L (not to scale in time). **b** Schematic charge stability diagram. The indicated points 'M' (measurement), 'T' (transfer), and 'R' (relaxation) are visited in the order and with the timing indicated in **a**. **c**–**j** Diagrams of the energy levels of the double quantum dot at each step of the pulse. In each dot, the lower (upper) level corresponds to the spin-down (spin-up) hole state. Numbers next to the label indicate the protocol step. **c** Emptying the right dot into the left dot. The arrows indicate the spin state of the left-dot orbitals; the right-dot orbitals are ordered likewise. **d** Ejecting the hole from the left dot into the lead to empty the system. **e**, **h** Injecting a hole in a random spin state into the left dot in the limiting case of $|L\Downarrow\rangle$ and $|L\Uparrow\rangle$, respectively. **f**, **i** Spin-selective transfer of the hole from left to right dot. **g**, **j** Latching the memory state into either the (0, 0) (**g**) or the (0, 1) configuration (**j**), and the detection of that state with the quantum point contact

(0, 1) configuration a long-lived excited state, while the configuration (0, 0) (empty memory register) is the ground state. In 2g and j, this situation is reflected by the fact that the two states of the right dot are above the Fermi energy of the left lead. However, the readout can also be performed if the M point were in the (0, 1) stability region. This would occur if in panels g and j the lowest-energy level of the right dot was below the Fermi energy level of the left lead. In such case, the filled memory register would constitute the ground state of the system, whereas the empty memory register would be in a latched excited state. Thus, the choice of the readout position should not have any influence on the outcome of our protocol.

Discussion

Since the transfer stage is the key element of our protocol, we examine the overall performance of the measurement as a function of the voltage ΔV_L at that stage. This voltage translates into an energy detuning ε between dot levels with the same spin. Figure 2f, i shows the system at $\varepsilon = -E_Z$. In this study, we choose $B = 1$ T and map out all possible alignments of levels of the left and right dot, from $\varepsilon < -E_Z$ to $\varepsilon > E_Z$, at the transfer stage. In this mapping, we preserve the overall shape of the pulse as in Fig. 2a, but move the three points, R, T, and M, along the line R–M toward the (0, 0) region (Fig. 2b). Figure 3a shows the memory state P_{01} averaged over 1000 measurements for two different times $T_R = 100$ ns (blue downward triangles) and 100 µs (red upward triangles) of the relaxation stage. We see a clear dependence of P_{01} on the time T_R, indicating that we are indeed sensitive to the evolution of the hole state caused by spin relaxation. However, the change ΔP_{01} of that probability, obtained as the difference between the two traces in Fig. 3a, strongly depends on the detuning ε, as shown in Fig. 3b. In the following, we focus on three alignments of levels, corresponding to $\varepsilon = -E_Z$, 0, and $+E_Z$, and depicted schematically in Fig. 3c–e, respectively. In the first case, the spin-up level of the left dot is in resonance with the spin-down level of the right dot, as also shown in Fig. 2f, i. As a result, only the spin-up component $|L\Uparrow\rangle$ of the hole in the left dot can transfer into the right dot, while the component $|L\Downarrow\rangle$ is lower in energy and therefore is blocked. Due to spin relaxation, the spin density $P_{L\Uparrow}(T_R)$ decreases as the relaxation time T_R increases, resulting in a decrease of the probability P_{01}, hence in a positive value of ΔP_{01}. We find that at this detuning our protocol operates with maximal sensitivity. On the other hand, at the detuning $\varepsilon = 0$ (Fig. 3d) the same-spin levels of the dots are on resonance and therefore the charge transfer process is not spin selective. As a result, here $\Delta P_{01} \approx 0$ (Fig. 3b), i.e, our protocol executed with $\varepsilon = 0$ is insensitive to the spin relaxation processes. Lastly, at the detuning $\varepsilon = E_Z$ (Fig. 3e), we again observe a resonant spin-selective alignment of states, in this case $|L\Downarrow\rangle$ and

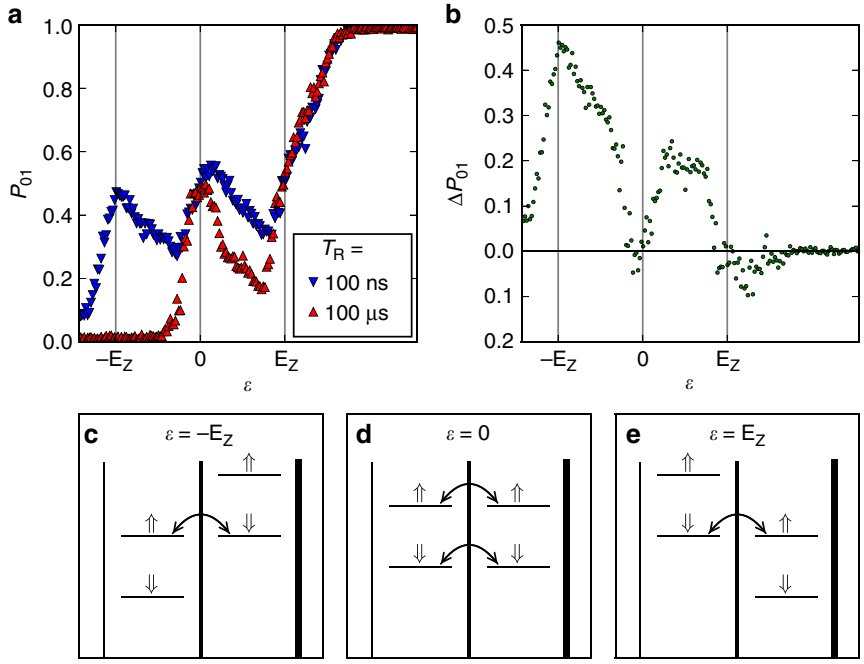

Fig. 3 Mapping the sensitivity of the protocol. **a** Average memory state P_{01} in 1000 measurements performed as a function of the detuning ε between the left and right dot in the transfer stage for two values of relaxation time T_R: 100 ns (blue downward triangles) and 100 µs (red upward triangles) at $B = 1$ T. **b** Sensitivity of the memory state P_{01} to the time T_R obtained as the difference between the traces in panel (**a**) . Panels **c**–**e** show schematically the energy diagrams of the system in the transfer stage at detunings $\varepsilon = -E_Z$, $\varepsilon = 0$, and $\varepsilon = E_Z$, respectively

$|R\Uparrow\rangle$. Here, one would expect that our protocol should detect the opposite spin component $|L\Downarrow\rangle$ of the left dot. This is indeed the case, as $\Delta P_{01} < 0$ close to that detuning, reflecting the relaxation induced increase of occupation of $|L\Downarrow\rangle$ with time T_R. However, at this alignment, the sensitivity is reduced. This is because during the pulse rise time the system passes across configurations $\varepsilon = -E_Z$ and $\varepsilon = 0$ undergoing, respectively, the spin-selective and spin-non-selective Landau–Zener tunneling process (see Supplementary Note 1). Also, at this alignment, multiple, non-resonant (inelastic) charge transfer channels are active and influence the state of the memory register. At detunings $\varepsilon > E_Z$, the probability P_{01} approaches unity for both relaxation times T_R due to the details of the pulsing sequence, as discussed in the Supplementary Note 1.

Next, we evaluate the fidelity of our spin measurement protocol at its maximum sensitivity. We define the fidelity of detection of the spin-up state $F_\Uparrow$ in terms of the conditional probability $P((0, 1)|L\Uparrow)$, i.e., probability that the memory register holds a hole on condition that the left-dot state was $|L\Uparrow\rangle$. Similarly, the fidelity of detection of the spin-down state is $F_\Downarrow = P((0, 0)|L\Downarrow)$. Based on the redistribution of probability densities after the transfer phase, we expect $F_\Downarrow \approx 1$; however, a similarly high $F_\Uparrow$ is unlikely due to the fact that the $|L\Uparrow\rangle$ state is mapped onto a distributed charge configuration. We confirm these expectations by a Bayesian analysis of our results (see Supplementary Notes 2 and 3), giving $F_\Downarrow = 0.99$ and $F_\Uparrow = 0.52$, and yielding the maximum visibility $V = F_\Uparrow + F_\Downarrow - 1 = 0.51$. We find that the portion $|L\Uparrow\rangle$ of the hole state after the relaxation phase is mapped in the transfer phase onto a roughly equal charge distribution in both dots, i.e., $P_{L\Uparrow}(T_R + T_T) \approx P_{R\Downarrow}(T_R + T_T)$. The fidelity $F_\Uparrow$ can be improved by replacing the constant voltage ΔV_L in the transfer phase of the protocol by a voltage pulse shaped to give $P_{L\Uparrow}(T_R + T_T) \approx 0$, e.g., with techniques similar to the adiabatic passage[49,51–55]. In the present version of the protocol, we optimized the duration of the transfer pulse for signal strength and range of magnetic fields. A longer transfer time reduces the upper limit of the magnetic field because it becomes comparable to T_1. A shorter transfer time, on the other hand, becomes comparable to the interdot resonance tunneling time (~20 ns).

In the unoptimized form, the protocol is expected to represent correctly the evolution of the hole state at the end of the relaxation phase as a function of T_R, provided that the relaxation time is the only parameter being adjusted. In Fig. 4a, we show single-shot measurements of the QPC current I_{QPC} at $B = 1$ T as a function of T_R revealing the state of the memory register. For short T_R, we find indications of both filled memory state (0, 1) (low QPC current), corresponding to the detection of the hole spin up, and empty memory state (0, 0) (high QPC current), corresponding to the detection of the hole spin down. On the other hand, for sufficiently long T_R, we find the memory register only in the empty state. In Fig. 4b, we show I_{QPC} obtained by Gaussian averaging of 1000 measurements for each T_R, showing a clear exponential profile. We reveal this profile by fitting to the relationship

$$I_{QPC}(T_R) = I_0 + I_1\left(1 - e^{-T_R/T_1}\right), \quad (1)$$

with I_0 and $I_0 + I_1$ corresponding to the filled and empty memory register, respectively. The fit shown with the solid black line is obtained with $T_1 = 2.8$ µs for $B = 1$ T.

In Fig. 4c, we show the dependence of the extracted relaxation time T_1 on the magnetic field. It follows the power law $T_1 = A \cdot B^{-N}$ with $A = 2.7 \pm 0.3$ µs and $N = 4.4 \pm 0.3$ (solid green line). Theoretical predictions of this dependence indicate two very different exponents, depending on the nature of the SOI[29,30]. The Dresselhaus SOI, arising as a result of the lack of inversion symmetry of the crystal lattice, is expected to give $N = 5$, while the Rashba SOI, brought about by the asymmetry of the sample geometry, should result in $N = 9$. The red-dashed line in Fig. 4c shows the fit with $N = 5$, indicating clearly that the spin relaxation in our system is dominated by the phonon-assisted Dresselhaus SOI. The theoretical exponent $N = 5$ is the lowest-order estimate only. Our results exhibit a deviation toward somewhat shorter values of

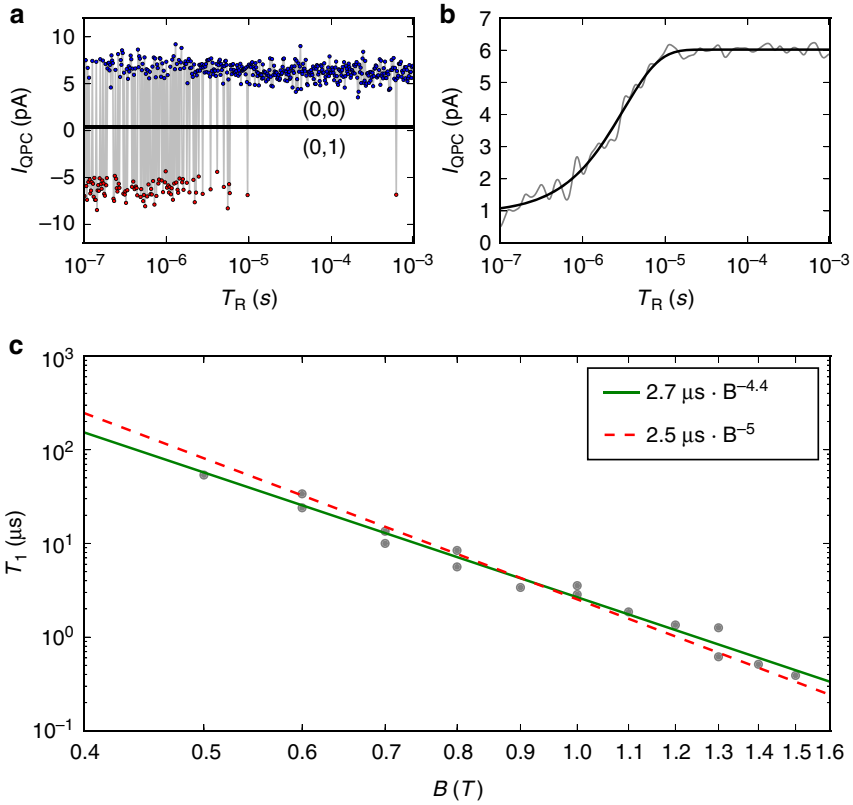

Fig. 4 Extraction of the spin relaxation time T_1. **a** Single-shot values of the charge detector current I_{QPC} revealing the state of the memory register as a function of the relaxation time T_R [high current corresponds to empty memory state (0,0)] at $B = 1$ T. **b** I_{QPC} as a function of T_R obtained by Gaussian averaging of multiple measurements. The solid line is a fit of the exponential population decay. The extracted value of spin relaxation time is $T_1 = 2.8$ μs. **c** Dependence of the spin relaxation time T_1 on the magnetic field. Lines show fits to a power law profile $T_1 = A \cdot B^{-N}$ with $N = 4.4$ (solid green) and $N = 5$ (dashed red)

T_1, particularly at lower magnetic fields. This is consistent with the recent optical measurements in self-assembled dots[56], where the dependence of T_1 on the magnetic field is more complex than a power law, and at low fields the theory overestimates the T_1 times as compared with the experimental values. This is likely due to the structural details of the quantum dot, which become less relevant at higher fields, when the cyclotron radius is smaller than the dot diameter and the system becomes more isotropic. We note that the values of T_1, ranging from ~400 ns at $B = 1.5$ T to ~60 μs at $B = 0.5$ T, are much longer than those measured to date in hole GaAs samples (e.g. ~300 ns at $B = 0.5$ T in ref. [38]), but shorter by an order of magnitude than those in Ge-based[34,35] or Si-based devices[37]. This is most likely due to the fact that centrosymmetric lattices such as Si do not exhibit the Dresselhaus SOI, leading to the dominance of the Rashba SOI in the spin relaxation mechanism. Also, our values of T_1 are about four orders of magnitude shorter than those in electronic GaAs dots at equivalent magnetic fields. Again, this is a consequence of much weaker SOI in the electronic systems[18,57–59] and a strongly elongated shape of our dot[48], which is known to enhance the spin–orbit coupling[21]. However, extrapolation of our values of T_1 to very low magnetic fields promises superior lifetime of the hole spin over that of the electron owing to the much weaker hyperfine interactions. Indeed, the record value of $T_1 = 57$ s reported in GaAs devices confining electrons[60] is limited by the isotropic hyperfine interaction between the electron spin and that of the nuclei, and depends on the magnetic field as B^{-3}. The hole exponent of $N \sim 5$ offers a more promising low-field scaling, and to date neither theoretical calculations[29,30], nor optical measurements[16,17,56] suggest any higher-order mechanisms leading to its deterioration.

Moreover, the hyperfine interaction in GaAs (as in all A_3B_5 materials) cannot be removed by isotopic purification. In our system, the hyperfine-mediated relaxation is not relevant, and the phonon-mediated spin–orbit relaxation is the dominant mechanism. The Dresselhaus SOI in A_3B_5 materials is unavoidable. However, we propose that the hole T_1 could be further extended by engineering the phonon density of states to eliminate the phonon modes mediating the spin–flip transitions. Preliminary work toward that end has already been demonstrated for electronic dots in nanowires[61].

Methods

Sample details. The experimental study was performed on a DQD fabricated from an undoped GaAs/$Al_xGa_{1-x}As$ ($x = 50\%$) heterostructure employing lateral split-gate technology[48–50]. A suitable DQD potential profile was defined by the deposited lateral Ti/Au gates. Holes were generated by a global gate deposited above the structure (not shown in Fig. 1a) separated by a 110-nm-thick Al_2O_3 dielectric layer grown by an atomic layer deposition technique. Left and right plunger gates, labeled as L and R, respectively, were used to tune the hole potentials individually in each dot, while the central gate was used to adjust the interdot tunneling barrier. The sample was cooled down in a dilution refrigerator at the nominal lattice temperature of 60 mK. The effective hole temperature, measured from the temperature dependence of the width at half maximum of a Coulomb blockade peak, was ~100 mK.

Experimental setup. The DC wiring of the Oxford Kelvinox-400 dilution refrigerator consisted of the following elements. It started with the pi-filters (Oxley pi-capacitors 5000 pf in combination with 470 Ohm in-series resistors) assembled in a copper box attached directly to the refrigerator. There are standard Cu–Ni twisted

pairs running from the room temperature top Fisher connector to a 1-K pot, followed by 60-cm-long, 0.5-mm-diameter thermo-coaxes (SS outer, Ni–Cr inner conductor, MnO dielectric) from the 1-K pot to the mixing chamber. A home-made loom of copper wires was used from the mixing chamber to the sample carrier to simultaneously cool the sample positioned in vacuum in the center of the 18-T superconducting solenoid. For high-frequency lines, we used 0.085″-diameter silver-plated Cu–Be semi-rigid coaxial cables with Anritsu V101 series connectors running from the room flange to the 1-K pot. Anritsu 20 dB attenuators were installed and thermo-anchored at the 1-K pot. Superconducting Nb coaxial cables were used from the 1-K pot to the mixing chamber to minimize the thermo-load. Modified Anritsu V251 bias-tees were installed and thermo-anchored at the mixing chamber followed by Ø 0.085″ copper semi-rigid coaxial cables down to the sample socket. In principle, the described radio-frequency wiring allows to deliver pulses with a sub-nanosecond rise time[62]. However, in the current experiments, we were limited by the sample design. In particular, in order to generate holes, our DQD sample had a relatively large global gate with increased parasitic capacitance to the ground that limited the bandwidth in current experiments to 100 MHz, or 10 ns rise time for pulses.

The charge state of the DQD was probed using a QPC charge sensor with a constant source-drain bias voltage of 100 μV. The measurement cycles were synchronized to the power line cycle by using the line trigger of the HP-3458A digital multimeter used to record the current readings. We independently exported the line trigger from our Tektronix TDS6154C oscilloscope and used it to trigger the arbitrary waveform generator. The rising edge of each power line cycle triggered both the pulse sequence and the reading. The charge state was measured by integrating the current I_{QPC} over one full period of the cycle: 1/60 Hz = 16.6(6) ms. Our setup could be modified to perform measurements in shorter cycles, however not reaching the sub-microsecond range.

Range of magnetic fields. Our measurements were performed in the magnetic-field range from ~0.4 T to ~1.6 T. The lower limit of the magnetic field is set by the condition of spin-selective resonant tunneling. For high protocol fidelity, the Zeeman gap between the left-dot levels has to be larger than the width of the resonance peaks shown in Fig. 3a. In our system, this occurs at $B \geq 0.4$ T, which corresponds to the Zeeman energy $E_Z \geq 30$ μeV. The upper limit of the magnetic field is defined by the value at which the spin relaxation time T_1 drops below the tunneling time constants set in our experiment, i.e., the length of the transfer step of 100 ns plus the minimum initialization time of 100 ns. At $B \sim 1.5$ T, these two times are of the same order as $T_1 \sim 400$ ns. However, both magnetic-field limits are more of technical than fundamental nature and can be extended by tuning the system parameters.

Data availability

The data that support the findings of this study are available from the corresponding author upon reasonable request.

Received: 31 August 2018 Accepted: 8 January 2019
Published online: 18 February 2019

References

1. Nielsen, M. A. & Chuang, I. L. *Quantum Computation and Quantum Information* (Cambridge University Press, Cambridge, 2010).
2. Henneberger, F. & Benson, O. *Semiconductor Quantum Bits* (Pan Stanford Publishing, Singapore, 2009).
3. Hanson, R., Kouwenhoven, L. P., Petta, J. R., Tarucha, S. & Vandersypen, L. M. K. Spins in few-electron quantum dots. *Rev. Mod. Phys.* **79**, 1217–1265 (2007).
4. De Greve, K. et al. Ultrafast coherent control and suppressed nuclear feedback of a single quantum dot hole qubit. *Nat. Phys.* **7**, 872–878 (2011).
5. Tartakovskii, A. Holes avoid decoherence. *Nat. Photonics* **5**, 647–649 (2011).
6. Coish, W. A., Golovach, V. N., Egues, J. C. & Loss, D. Measurement, control, and decay of quantum-dot spins. *Phys. Stat. Sol. (B)* **243**, 3658–3672 (2006).
7. Petta, J. R. et al. Pulsed-gate measurements of the singlet-triplet relaxation time in a two-electron double quantum dot. *Phys. Rev. B* **72**, 161301 (2005).
8. Tyryshkin, A. M. et al. Electron spin coherence exceeding seconds in high-purity silicon. *Nat. Mater.* **11**, 143–147 (2011).
9. Testelin, C., Bernardot, F., Eble, B. & Chamarro, M. Hole–spin dephasing time associated with hyperfine interaction in quantum dots. *Phys. Rev. B* **79**, 195440 (2009).
10. Wang, X. J., Chesi, S. & Coish, W. A. Spin-echo dynamics of a heavy hole in a quantum dot. *Phys. Rev. Lett.* **109**, 237601 (2012).
11. Fischer, J., Coish, W. A., Bulaev, D. V. & Loss, D. Spin decoherence of a heavy hole coupled to nuclear spins in a quantum dot. *Phys. Rev. B* **78**, 155329 (2008).
12. Burkard, G. Positively spin coherent. *Nat. Mater.* **7**, 100–101 (2008).
13. Fallahi, P., Yilmaz, S. T. & Imamoğlu, A. Measurement of a heavy-hole hyperfine interaction in InGaAs quantum dots using resonance fluorescence. *Phys. Rev. Lett.* **105**, 257402 (2010).
14. Chekhovich, E. A., Krysa, A. B., Skolnick, M. S. & Tartakovskii, A. I. Direct measurement of the hole-nuclear spin interaction in single InP/GaInP quantum dots using photoluminescence spectroscopy. *Phys. Rev. Lett.* **106**, 027402 (2011).
15. Carter, S. G. et al. Strong hyperfine-induced modulation of an optically driven hole spin in an inas quantum dot. *Phys. Rev. B* **89**, 075316 (2014).
16. Greilich, A., Carter, S. G., Kim, D., Bracker, A. S. & Gammon, D. Optical control of one and two hole spins in interacting quantum dots. *Nat. Photonics* **5**, 702–708 (2011).
17. Gerardot, B. D. et al. Optical pumping of a single hole spin in a quantum dot. *Nature* **451**, 441–444 (2008).
18. Nadj-Perge, S. et al. Disentangling the effects of spin-orbit and hyperfine interactions on spin blockade. *Phys. Rev. B* **81**, 201305 (2010).
19. Prance, J. R. et al. Single-shot measurement of triplet-singlet relaxation in a Si/SiGe double quantum dot. *Phys. Rev. Lett.* **108**, 046808 (2012).
20. Simmons, C. B. et al. Tunable spin loading and T_1 of a silicon spin qubit measured by single-shot readout. *Phys. Rev. Lett.* **106**, 156804 (2011).
21. Amasha, S. et al. Electrical control of spin relaxation in a quantum dot. *Phys. Rev. Lett.* **100**, 046803 (2008).
22. Kroutvar, M. et al. Optically programmable electron spin memory using semiconductor quantum dots. *Nature* **432**, 81–84 (2004).
23. Fujisawa, T., Austing, D. G., Tokura, Y., Hirayama, Y. & Tarucha, S. Allowed and forbidden transitions in artificial hydrogen and helium atoms. *Nature* **419**, 278–281 (2002).
24. Golovach, V. N., Khaetskii, A. & Loss, D. Phonon-induced decay of the electron spin in quantum dots. *Phys. Rev. Lett.* **93**, 016601 (2004).
25. Khaetskii, A. V. & Nazarov, Y. V. Spin-flip transitions between zeeman sublevels in semiconductor quantum dots. *Phys. Rev. B* **64**, 125316 (2001).
26. Hanson, R. et al. Single-shot readout of electron spin states in a quantum dot using spin-dependent tunnel rates. *Phys. Rev. Lett.* **94**, 196802 (2005).
27. Meunier, T. et al. Experimental signature of phonon-mediated spin relaxation in a two-electron quantum dot. *Phys. Rev. Lett.* **98**, 126601 (2007).
28. Elzerman, J. M. et al. Single-shot read-out of an individual electron spin in a quantum dot. *Nature* **430**, 431–435 (2004).
29. Bulaev, D. V. & Loss, D. Spin relaxation and decoherence of holes in quantum dots. *Phys. Rev. Lett.* **95**, 076805 (2005).
30. Bulaev, D. V. & Loss, D. Electric dipole spin resonance for heavy holes in quantum dots. *Phys. Rev. Lett.* **98**, 097202 (2007).
31. Woods, L. M., Reinecke, T. L. & Kotlyar, R. Hole spin relaxation in quantum dots. *Phys. Rev. B* **69**, 125330 (2004).
32. Lü, C., Cheng, J. L. & Wu, M. W. Hole spin relaxation in semiconductor quantum dots. *Phys. Rev. B* **71**, 075308 (2005).
33. Climente, J. I., Segarra, C. & Planelles, J. Spin-orbit-induced hole spin relaxation in InAs and GaAs quantum dots. *New J. Phys.* **15**, 093009 (2013).
34. Hu, Y., Kuemmeth, F., Lieber, C. M. & Marcus, C. M. Hole spin relaxation in Ge-Si core-shell nanowire qubits. *Nat. Nanotechnol.* **7**, 47–50 (2012).
35. Higginbotham, A. P. et al. Hole spin coherence in a Ge/Si heterostructure nanowire. *Nano Lett.* **14**, 3582–3586 (2014).
36. Vukusic, L. et al. Single-shot readout of hole spins in Ge. *Nano Lett.* **18**, 7141–7145 (2018).
37. Bohuslavskyi, H. et al. Pauli blockade in a few-hole PMOS double quantum dot limited by spin-orbit interaction. *Appl. Phys. Lett.* **109**, 193101 (2016).
38. Wang, D. Q. et al. Anisotropic Pauli spin blockade of holes in a GaAs double quantum dot. *Nano Lett.* **16**, 7685–7689 (2016).
39. Watzinger, H. et al. A germanium hole spin qubit. *Nat. Commun.* **9**, 3902 (2018).
40. Maurand, R. et al. A CMOS silicon spin qubit. *Nat. Commun.* **7**, 13575 (2016).
41. Siddiqi, I. et al. Dispersive measurements of superconducting qubit coherence with a fast latching readout. *Phys. Rev. B* **73**, 054510 (2006).
42. Studenikin, S. A. et al. Enhanced charge detection of spin qubit readout via an intermediate state. *Appl. Phys. Lett.* **101**, 233101 (2012).
43. Fogarty, M. A. et al. Integrated silicon qubit platform with single-spin addressability, exchange control and robust single-shot singlet-triplet readout. *Nat. Commun.* **9**, 4370 (2018).
44. Harvey-Collard, P. et al. High-fidelity single-shot readout for a spin qubit via an enhanced latching mechanism. *Phys. Rev. X* **8**, 021046 (2018).
45. Nakajima, T. et al. Robust single-shot spin measurement with 99.5% fidelity in a quantum dot array. *Phys. Rev. Lett.* **119**, 017701 (2017).
46. Orona, L. A. et al. Readout of singlet-triplet qubits at large magnetic field gradients. *Phys. Rev. B* **98**, 125404 (2018).
47. Pfund, A., Shorubalko, I., Ensslin, K. & Leturcq, R. Suppression of spin relaxation in an inas nanowire double quantum dot. *Phys. Rev. Lett.* **99**, 036801 (2007).
48. Bogan, A. et al. Consequences of spin-orbit coupling at the single hole level: spin-flip tunneling and the anisotropic *g* factor. *Phys. Rev. Lett.* **118**, 167701 (2017).

49. Bogan, A. et al. Landau-Zener-Stückelberg-Majorana interferometry of a single hole. *Phys. Rev. Lett.* **120**, 207701 (2018).
50. Tracy, L. A., Hargett, T. W. & Reno, J. L. Few-hole double quantum dot in an undoped GaAs/AlGaAs heterostructure. *Appl. Phys. Lett.* **104**, 123101 (2014).
51. Petta, J. R., Johnson, A. C., Marcus, C. M., Hanson, M. P. & Gossard, A. C. Manipulation of a single charge in a double quantum dot. *Phys. Rev. Lett.* **93**, 186802 (2004).
52. Sánchez, R. et al. Long-range spin transfer in triple quantum dots. *Phys. Rev. Lett.* **112**, 176803 (2014).
53. Greentree, A. D., Cole, J. H., Hamilton, A. R. & Hollenberg, L. C. L. Coherent electronic transfer in quantum dot systems using adiabatic passage. *Phys. Rev. B* **70**, 235317 (2004).
54. Busl, M. et al. Bipolar spin blockade and coherent state superpositions in a triple quantum dot. *Nat. Nanotechnol.* **8**, 261–265 (2013).
55. Braakman, F. R., Barthelemy, P., Reichl, C., Wegscheider, W. & Vandersypen, L. M. Long-distance coherent coupling in a quantum dot array. *Nat. Nanotechnol.* **8**, 432–437 (2013).
56. Heiss, D. et al. Observation of extremely slow hole spin relaxation in self-assembled quantum dots. *Phys. Rev. B* **76**, 241306(R) (2007).
57. Nichol, J. M. et al. Quenching of dynamic nuclear polarization by spinorbit coupling in GaAs quantum dots. *Nat. Commun.* **6**, 7682 (2015).
58. Fujita, T. et al. Signatures of hyperfine, spin-orbit, and decoherence effects in a Pauli spin blockade. *Phys. Rev. Lett.* **117**, 206802 (2016).
59. Maisi, V. F. et al. Spin-orbit coupling at the level of a single electron. *Phys. Rev. Lett.* **116**, 136803 (2016).
60. Camenzind, L. C. et al. Hyperfine-phonon spin relaxation in a single-electron GaAs quantum dot. *Nat. Commun.* **9**, 3454 (2018).
61. Wang, M., Yin, Y. & Wu, M. W. Electric manipulation of electron spin relaxation induced by confined phonons in nanowire-based double quantum dots. *J. Appl. Phys.* **109**, 103713 (2007).
62. Korkusinski, M. et al. Landau-Zener-Stückelberg Interferometry in quantum dots with fast rise times: evidence for coherent phonon driving. *Phys. Rev. Lett.* **118**, 067701 (2017).

Acknowledgments

A.B. and S.S. thanks the Natural Sciences and Engineering Research Council of Canada for financial support. This work was performed in part at the Center for Integrated Nanotechnologies, a U.S. DOE, Office of Basic Energy Sciences user facility, and Sandia National Laboratories, a multi-mission laboratory managed and operated by National Technology and Engineering Solutions of Sandia, LLC., a wholly owned subsidiary of Honeywell International, Inc., for the U.S. Department of Energy's National Nuclear Security Administration under contract DE-NA-0003525. Any subjective views or opinions that might be expressed in the paper do not necessarily represent the views of the U.S. Department of Energy or the United States Government.

Author contributions

A.B. and S.S. performed the measurements, A.B., S.S., M.K., L.G. and A.S.S. analyzed the data, A.B. and M.K. wrote the paper, P.Z. provided maintenance of the cryogenic and measurement equipment, L.T., J.R. and T.H. created and characterized the sample.

Additional information

Supplementary information accompanies this paper at https://doi.org/10.1038/s42005-019-0113-0.

Competing interests: The authors declare no competing interests.

Reprints and permission information is available online at http://npg.nature.com/reprintsandpermissions/

Publisher's note: Springer Nature remains neutral with regard to jurisdictional claims in published maps and institutional affiliations.

Open Access This article is licensed under a Creative Commons Attribution 4.0 International License, which permits use, sharing, adaptation, distribution and reproduction in any medium or format, as long as you give appropriate credit to the original author(s) and the source, provide a link to the Creative Commons license, and indicate if changes were made. The images or other third party material in this article are included in the article's Creative Commons license, unless indicated otherwise in a credit line to the material. If material is not included in the article's Creative Commons license and your intended use is not permitted by statutory regulation or exceeds the permitted use, you will need to obtain permission directly from the copyright holder. To view a copy of this license, visit http://creativecommons.org/licenses/by/4.0/.

© The Author(s) 2019